Hybrid-Mode Analysis of Planar Transmission Lines with Arbitrary Metallization Cross Sections

Zhewang Ma, Eikichi Yamashita, *Fellow, IEEE*, and Shanjia Xu, *Senior Member, IEEE*

Abstract—**The problem of planar transmission lines of arbitrary metallization cross sections is solved by using the generalized transverse resonance technique combined with the mode-matching procedure. Analyses are carried out on the dispersion characteristics of microstrip lines, finlines and coplanar waveguides with trapezoidal strip cross sections. Numerical results verify the versatility and accuracy of this method, and show that the profiles of the metallizations in miniaturized MMIC guiding structures give marked effects on the transmission properties.**

I. Introduction

THE CONTINUING process in microwave monolithic integrated circuits (MMIC's) is towards higher frequencies, higher component densities, smaller miniaturized circuit sizes, and the development of higher performance components with increasing complexity. As a result of improvements in fabrication technology, the design of MMIC's demands more accurate modeling of practically used waveguiding structures, and consequently some of the approximations employed in the computer aided design (CAD) of microwave circuits become no longer useful. In particular, due to the very narrow strip width used in the MMIC's [1]–[6], the exact profile of the conductor strip should be considered to characterize exactly the transmission properties of the planar waveguides. Actually, a variety of complicated cross sections are exhibited in active and passive MMIC waveguiding structures which are neither of planar nor of rectangular geometry. For example, because of the occurrence of underetching or electrolytical growth during fabrication, the cross section of the strip is likely to be better approximated by a trapezoid than by a rectangle [1]–[3]. Although the effect of the metallization thickness on the transmission properties of planar transmission lines has been discussed in some papers [7]–[9], most are restricted to the cases where the conductor strips have rectangular cross sections. Only very recently has the more general problem of a microstrip with arbitrary conductor cross section been treated [1]–[3].

The flexibility of the finite element method (FEM) and the finite difference method (FDM) may be used to deal with arbitrary conductor cross-sections. But these methods require large computer memory as well as time-consuming computations [1]–[3]. The mode-matching method has been shown to be a very versatile and effective method for a variety of electromagnetic problems [7]–[12]. However, to the authors' knowledge, this method has not so far been applied to planar waveguides with arbitrary metallization

In this contribution, based on the mode-matching procedure, the dispersion analysis of planar waveguides of arbitrary perfect conductor cross-sections is presented by using the step approximation of the conductor profile and the transverse resonance techniques. As examples, the dispersion characteristics of microstrip lines of rectangular and trapezoidal strip cross sections are calculated, and comparison, where possible, is made with results by other authors. For the first time, provided are the propagation constants of finlines and coplanar waveguides with trapezoidal metallization cross sections, and a comparison between the effects of the conductor thickness and the conductor geometry on the propagation constants of coplanar waveguides.

II. Formulation of the Problem

Fig. 1 shows a generalized planar waveguiding structure. It consists of an arbitrary number of metallic strips deposited on various dielectric substrate interfaces. In this analysis, the arbitrary profiles of metallic strips are approximated by a series of small steps, as shown in Fig. 2. In general, the fields in the dielectric slab-loaded, ridged waveguide may be expressed as a superposition of the LSE and LSM modes with respect to the z-direction (i.e., the TE and TM modes with respect to the y-direction). Following the conventional transverse resonance procedure [7]–[9], we consider that the LSE and LSM modes propagate in the transverse direction and couple each other at discontinuities of various vertical planes. The hybrid modes as waveguide fields are formed as a result of repeated reflections of the LSE and LSM mode waves at short or open-circuited ends and discontinuities. Thus, at first we derive the scattering matrix of the N-furcated waveguide junction as shown in Fig. 3 for the LSE and LSM mode excitation, then we use the generalized scattering matrix technique to obtain the overall scattering matrix of the cascaded discontinuities, and finally we formulate the eigenvalue equation for the propagation constant by using the transverse resonance condition.

A. Treatment of the N-Furcated Waveguide Junction

The hybrid mode fields, $\boldsymbol{E}$ and $\boldsymbol{H}$, are derived from the electric- and magnetic-type Hertzian potential functions, $\boldsymbol{\Pi}^e$

Manuscript received April 9, 1992; revised July 9, 1992.

Z. Ma and E. Yamashita are with the Department of Electronic Engineering, University of Electro-communications, Chofugaoka 1-5-1, Chofu-shi, Tokyo 182, Japan.

S. Xu is with the University of Science and Technology of China, Hefei, Anhui 230026, P.R. China.

IEEE Log Number 9205457.

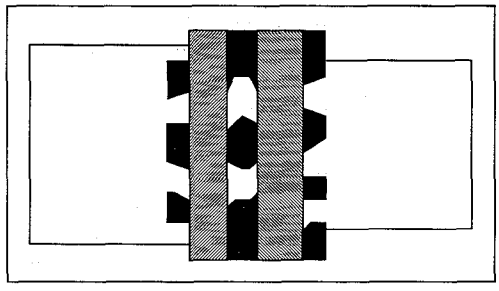

Fig. 1. A generalized planar guiding structure.

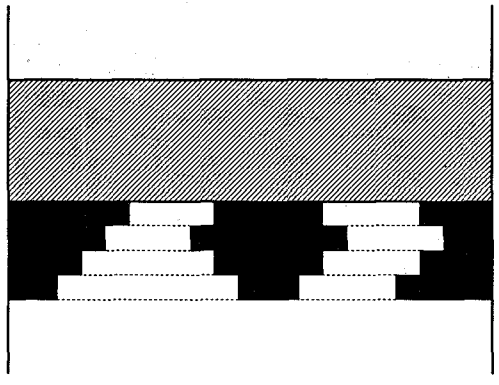

Fig. 2. Step approximation of an arbitrary metallization profile.

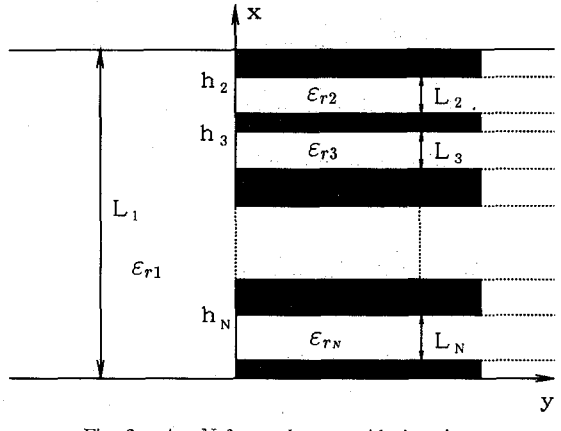

Fig. 3. An N-furcated waveguide junction.

and $\boldsymbol{\Pi}^h$, as follows:

$$\boldsymbol{E} = \nabla \times \nabla \times \boldsymbol{\Pi}^e - j\omega\mu\nabla \times \boldsymbol{\Pi}^h \tag{1}$$

$$\boldsymbol{H} = \nabla \times \nabla \times \boldsymbol{\Pi}^h + j\omega\varepsilon\nabla \times \boldsymbol{\Pi}^e \tag{2}$$

Appropriate solutions for $\boldsymbol{\Pi}^h$ and $\boldsymbol{\Pi}^e$ in the ith waveguide are derived by using the method of the separation of variables and are given by

$$\boldsymbol{\Pi}^h_{in} = \frac{C^h_{in}}{j\sqrt{\omega\mu k^h_{yin}}} \cos k^h_{xin} \cdot (x - h_i) e^{-jk^h_{yin} y} e^{-jk_z z} \boldsymbol{i}_y \tag{3}$$

$$\boldsymbol{\Pi}^e_{in} = \frac{C^e_{in}}{j\sqrt{\omega\varepsilon_0\varepsilon_{ri} k^e_{yin}}} \sin k^e_{xin} \cdot (x - h_i) e^{-jk^e_{yin} y} e^{-jk_z z} \boldsymbol{i}_y \tag{4}$$

and the transverse components (with respect to the y-direction) of the fields are then expressed as

$$\boldsymbol{e}^h_{in} = \sqrt{Z^h_{in}} C^h_{in} (-jk_z \cos k^h_{xin}(x - h_i)\boldsymbol{i}_x + k^h_{xin} \sin k^h_{xin}(x - h_i)\boldsymbol{i}_z) e^{-jk_z z} \tag{5a}$$

$$\boldsymbol{h}^h_{in} = \sqrt{Y^h_{in}} C^h_{in} (k^h_{xin} \sin k^h_{xin}(x - h_i)\boldsymbol{i}_x + jk_z \cos k^h_{xin}(x - h_i)\boldsymbol{i}_z) e^{-jk_z z} \tag{5b}$$

$$\boldsymbol{e}^e_{in} = \sqrt{Z^e_{in}} C^e_{in} (-k^e_{xin} \cos k^e_{xin}(x - h_i)\boldsymbol{i}_x + jk_z \sin k^e_{xin}(x - h_i)\boldsymbol{i}_z) e^{-jk_z z} \tag{5c}$$

$$\boldsymbol{h}^e_{in} = \sqrt{Y^e_{in}} C^e_{in} (jk_z \sin k^e_{xin}(x - h_i)\boldsymbol{i}_x + k^e_{xin} \cos k^e_{xin}(x - h_i)\boldsymbol{i}_z) e^{-jk_z z} \tag{5d}$$

where

$$k^{h,e}_{in} = \frac{n\pi}{L_i},$$

$$\cdot (k^{h,e}_{cin})^2 = (k^{h,e}_{xin})^2 + (k_z)^2,$$

$$\cdot (k^{h,e}_{yin})^2 = \omega^2\mu\varepsilon_0\varepsilon_{ri} - (k^{h,e}_{cin})^2$$

$$Z^h_{in} = \frac{1}{Y^h_{in}} = \frac{\omega\mu}{k^h_{yin}},$$

$$Z^e_{in} = \frac{1}{Y^e_{in}} = \frac{k^e_{yin}}{\omega\varepsilon_0\varepsilon_{ri}}$$

$$C^h_{in} = \sqrt{\frac{2}{1 + \delta_{on}}} \frac{1}{k^h_{cin}\sqrt{L_i}},$$

$$C^e_{in} = \frac{\sqrt{2}}{k^e_{cin}\sqrt{L_i}}$$

$$\delta_{on} = \begin{cases} 1 & \text{if } n = 0 \\ 0 & \text{if } n \neq 0 \end{cases},$$

$$n = \begin{cases} 0, 1, 2, \cdots \text{ for LSE mode} \\ 1, 2, 3, \cdots \text{ forLSM mode} \end{cases}$$

If the vector-mode functions, $\tilde{\boldsymbol{e}}_{in}$ and $\tilde{\boldsymbol{h}}_{in}$, are defined by replacing k_z with $-k_z$ in (5a)–(5d) [10], the following orthonormality relations are satisfied

$$\int_{h_i - L_i}^{h_i} \boldsymbol{e}^h_{in} \times \tilde{\boldsymbol{h}}^h_{im} \cdot \boldsymbol{i}_y \, dx = \int_{h_i - L_i}^{h_i} \tilde{\boldsymbol{e}}^h_{in} \times \boldsymbol{h}^h_{im} \cdot \boldsymbol{i}_y \, dx = \delta_{nm} \tag{6a}$$

$$\int_{h_i - L_i}^{h_i} \boldsymbol{e}^e_{in} \times \tilde{\boldsymbol{h}}^e_{im} \cdot \boldsymbol{i}_y \, dx = \int_{h_i - L_i}^{h_i} \tilde{\boldsymbol{e}}^e_{in} \times \boldsymbol{h}^e_{im} \cdot \boldsymbol{i}_y \, dx = \delta_{nm} \tag{6b}$$

$$\int_{h_i - L_i}^{h_i} \boldsymbol{e}^h_{in} \times \tilde{\boldsymbol{h}}^e_{im} \cdot \boldsymbol{i}_y \, dx = \int_{h_i - L_i}^{L_i} \tilde{\boldsymbol{e}}^h_{in} \times \boldsymbol{h}^e_{im} \cdot \boldsymbol{i}_y \, dx = 0 \tag{6c}$$

$$\int_{h_i - L_i}^{h_i} \boldsymbol{e}^e_{in} \times \tilde{\boldsymbol{h}}^h_{im} \cdot \boldsymbol{i}_y \, dx = \int_{h_i - L_i}^{h_i} \tilde{\boldsymbol{e}}^e_{in} \times \boldsymbol{h}^h_{im} \cdot \boldsymbol{i}_y \, dx = 0 \tag{6d}$$

where δ_{nm} is the Kronecker delta (= 1 if $n = m$; = 0 if $n \neq m$). In the lossless case, k_z is purely real for propagating modes. According to the definition of the tilded-mode functions and to (5), it is evident that when no loss is present the tilded-mode functions are the complex conjugates of those in (5).

Now the electric and magnetic fields in the ith guide at $z = 0$ may be expanded in an infinite sum of LSE- and LSM-mode components as

$$\begin{aligned}\boldsymbol{E}_{it}(x,y) = &\sum_{n=0,1,2,\cdots}(A^h_{in}e^{-jk^h_{y_{in}}y} + B^h_{in}e^{jk^h_{y_{in}}y})\boldsymbol{e}^h_{in}(x)\\ &+\sum_{n=1,2,3\cdots}(A^e_{in}e^{-jk^e_{y_{in}}y} + B^e_{in}e^{jk^e_{y_{in}}y}\\ &+ B^e_{in}e^{jk^h_{y_{in}}y})\boldsymbol{e}^e_{in}(x) \qquad (7)\\ \boldsymbol{H}_{it}(x,y) = &\sum_{n=0,1,2,\cdots}(A^h_{in}e^{-jk^h_{y_{in}}y} - B^h_{in}e^{jk^e_{y_{in}}y})\boldsymbol{h}^h_{in}(x)\\ &+\sum_{n=1,2,3,\cdots}(A^e_{in}e^{-jk^e_{y_{in}}y} - B^e_{in}e^{jk^e_{y_{in}}y})\boldsymbol{h}^e_{in}(x) \qquad (8)\end{aligned}$$

where the coefficients, A_{in} and B_{in}, represent the amplitudes of the incident and reflected (with respect to the y-direction) waves in the ith guide. Using the boundary conditions at $y = 0$ and $z = 0$ and matching the tangential fields, $\boldsymbol{E}_{it}$ and $\boldsymbol{H}_{it}$, lead to a pair of equations on the tangential components of electromagnetic fields. Vector-multiplying the electric component vector equation successively by $\tilde{\boldsymbol{h}}^h_{1m}$ and $\tilde{\boldsymbol{h}}^e_{1m}$, and the magnetic component vector equation successively by $\tilde{\boldsymbol{e}}^h_{im}$ and $\tilde{\boldsymbol{e}}^e_{im}$, using the orthonormality relation (6) and taking truncation on both sides of these equations, we get a set of linear simultaneous equations in the following matrix form:

$$\begin{bmatrix}\boldsymbol{A}^h_1 + \boldsymbol{B}^h_1\\ \boldsymbol{A}^e_1 + \boldsymbol{B}^e_1\end{bmatrix} = \begin{bmatrix}\boldsymbol{R}^{hh}_{12} & \boldsymbol{R}^{he}_{12} & \cdots & \boldsymbol{R}^{hh}_{1N} & \boldsymbol{R}^{he}_{1N}\\ \boldsymbol{R}^{eh}_{12} & \boldsymbol{R}^{ee}_{12} & \cdots & \boldsymbol{R}^{eh}_{1N} & \boldsymbol{R}^{ee}_{1N}\end{bmatrix} \cdot \begin{bmatrix}\boldsymbol{A}^h_2 + \boldsymbol{B}^h_2\\ \boldsymbol{A}^e_2 + \boldsymbol{B}^e_2\\ \vdots\\ \boldsymbol{A}^h_N + \boldsymbol{B}^h_N\\ \boldsymbol{A}^e_N + \boldsymbol{B}^e_N\end{bmatrix}$$

$$= [\boldsymbol{R}]\begin{bmatrix}\boldsymbol{A}^h_2 + \boldsymbol{B}^h_2\\ \boldsymbol{A}^e_2 + \boldsymbol{B}^e_2\\ \vdots\\ \boldsymbol{A}^h_N + \boldsymbol{B}^h_N\\ \boldsymbol{A}^e_N + \boldsymbol{B}^e_N\end{bmatrix} \qquad (9)$$

$$\cdot\begin{bmatrix}\boldsymbol{B}^h_2 - \boldsymbol{A}^h_2\\ \boldsymbol{B}^e_2 - \boldsymbol{A}^e_2\\ \vdots\\ \boldsymbol{B}^h_N - \boldsymbol{A}^h_N\\ \boldsymbol{B}^e_N - \boldsymbol{A}^e_N\end{bmatrix} = \begin{bmatrix}\boldsymbol{H}^{hh}_{12} & \boldsymbol{H}^{eh}_{12}\\ \boldsymbol{H}^{he}_{12} & \boldsymbol{H}^{ee}_{12}\\ \vdots & \vdots\\ \boldsymbol{H}^{hh}_{1N} & \boldsymbol{H}^{eh}_{1N}\\ \boldsymbol{H}^{he}_{1N} & \boldsymbol{H}^{ee}_{1N}\end{bmatrix}$$

$$\cdot\begin{bmatrix}\boldsymbol{A}^h_1 - \boldsymbol{B}^h_1\\ \boldsymbol{A}^e_1 - \boldsymbol{B}^e_1\end{bmatrix} = [H]\begin{bmatrix}\boldsymbol{A}^h_1 - \boldsymbol{B}^h_1\\ \boldsymbol{A}^e_1 - \boldsymbol{B}^e_1\end{bmatrix} \qquad (10)$$

where

$$\begin{aligned}(\boldsymbol{R}^{hh}_{1i})_{mn} &= \int_{h_i-L_i}^{h_i}\boldsymbol{e}^h_{in}\times\tilde{\boldsymbol{h}}^h_{1m}\cdot\boldsymbol{i}_y\,dx,\\ (\boldsymbol{R}^{he}_{1i})_{mn} &= \int_{h_i-L_i}^{h_i}\boldsymbol{e}^e_{in}\times\tilde{\boldsymbol{h}}^h_{1m}\cdot\boldsymbol{i}_y\,dx\\ (\boldsymbol{R}^{eh}_{1i})_{mn} &= \int_{h_i-L_i}^{h_i}\boldsymbol{e}^h_{in}\times\tilde{\boldsymbol{h}}^e_{1m}\cdot\boldsymbol{i}_y\,dx,\\ (\boldsymbol{R}^{ee}_{1i})_{mn} &= \int_{h_i-L_i}^{h_i}\boldsymbol{e}^e_{in}\times\tilde{\boldsymbol{h}}^e_{1m}\cdot\boldsymbol{i}_y\,dx\\ (\boldsymbol{H}^{hh}_{1i})_{mn} &= \int_{h_i-L_i}^{h_i}\tilde{\boldsymbol{e}}^h_{im}\times\boldsymbol{h}^h_{1n}\cdot\boldsymbol{i}_y\,dx\\ &= (\boldsymbol{R}^{hh}_{1i})_{nm}\\ (\boldsymbol{H}^{he}_{1i})_{mn} &= \int_{h_i-L_i}^{h_i}\tilde{\boldsymbol{e}}^e_{im}\times\boldsymbol{h}^h_{1n}\cdot\boldsymbol{i}_y\,dx\\ &= (\tilde{\boldsymbol{R}}^{he}_{1i})_{nm}\\ (\boldsymbol{H}^{eh}_{1i})_{mn} &= \int_{h_i-L_i}^{h_i}\tilde{\boldsymbol{e}}^h_{im}\times\boldsymbol{h}^e_{1n}\cdot\boldsymbol{i}_y\,dx\\ &= (\tilde{\boldsymbol{R}}^{eh}_{1i})_{nm}\\ (\boldsymbol{H}^{ee}_{1i})_{mn} &= \int_{h_i-L_i}^{h_i}\tilde{\boldsymbol{e}}^e_{im}\times\boldsymbol{h}^e_{1n}\cdot\boldsymbol{i}_y\,dx\\ &= (\boldsymbol{R}^{ee}_{1i})_{nm}\\ i &= 2,3,\cdots,N\end{aligned}$$

As all the space vector mode-functions in the above integral are the combinations of sine and cosine functions, the integrations can be analytically carried out easily. The tilded functions $(\tilde{\boldsymbol{R}}^{he}_{1i})_{nm}$ and $(\tilde{\boldsymbol{R}}^{eh}_{1i})_{nm}$ are also defined by replacing k_z with $-k_z$ in $(\boldsymbol{R}^{he}_{1i})_{nm}$, respectively. From (9) and (10), it is not difficult to deduce the scattering matrix $\boldsymbol{S}$ of the N-furcated junction in a form as shown below

$$\begin{bmatrix}\boldsymbol{B}^h_1\\ \boldsymbol{B}^e_1\\ \vdots\\ \boldsymbol{B}^h_N\\ \boldsymbol{B}^e_N\end{bmatrix} = \begin{bmatrix}\boldsymbol{S}_{11} & \boldsymbol{S}_{12}\\ \boldsymbol{S}_{21} & \boldsymbol{S}_{22}\end{bmatrix}\begin{bmatrix}\boldsymbol{A}^h_1\\ \boldsymbol{A}^e_1\\ \vdots\\ \boldsymbol{A}^h_N\\ \boldsymbol{A}^e_N\end{bmatrix} \qquad (11)$$

where

$$\begin{aligned}\boldsymbol{S}_{22} &= (\boldsymbol{I}+\boldsymbol{HR})^{-1}(\boldsymbol{I}-\boldsymbol{HR})\\ &= 2(\boldsymbol{I}+\boldsymbol{HR})^{-1} - \boldsymbol{I} \qquad (12a)\\ \boldsymbol{S}_{21} &= 2(\boldsymbol{I}+\boldsymbol{HR})^{-1}\boldsymbol{H} = (\boldsymbol{S}_{22}+\boldsymbol{I})\boldsymbol{H} \qquad (12b)\\ \boldsymbol{S}_{12} &= 2\boldsymbol{R}(\boldsymbol{I}+\boldsymbol{HR})^{-1} = \boldsymbol{R}(\boldsymbol{S}_{22}+\boldsymbol{I}) \qquad (12c)\\ \boldsymbol{S}_{11} &= \boldsymbol{S}_{12}\boldsymbol{H} - \boldsymbol{I} = \boldsymbol{RS}_{21} - \boldsymbol{I} \qquad (12d)\end{aligned}$$

B. Cascaded Discontinuities

In the case of cascaded discontinuities, there are two approaches. The first is to combine the transmission matrices of individual discontinuities for expressing the overall transmission matrix, and it requires an equal number of modes in any of the sections connecting discontinuities. As is well known, however, the mode-matching analysis usually requires

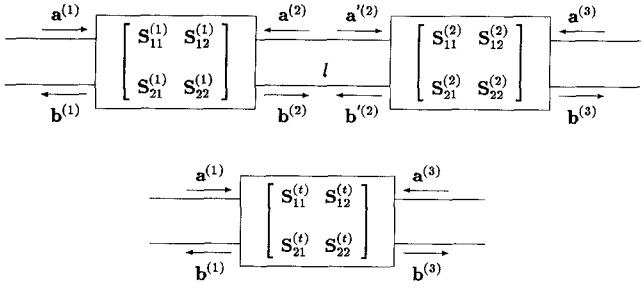

Fig. 4. Scattering matrix representation of cascaded discontinuities.

a proper choice of the number of modal terms retained in the guides connected to the junction to overcome the relative convergence problem [11], [12], and it has been shown in [11] that the requirement of an equal number of modal terms in any of the sections may violate the edge condition, resulting in incorrect numerical solutions. Thus, in this paper the cascaded discontinuity problems are treated by using the second approach, i.e., the generalized scattering matrix method [12].

Referring to Fig. 4, the sub-matrices of the overall scattering matrix (superscript t) of two cascaded junctions, separated by a uniform line section of length l, are given by

$$S_{11}^{(t)} = S_{11}^{(1)} + S_{12}^{(1)} DES_{11}^{(2)} DS_{21}^{(1)} \tag{13a}$$

$$S_{12}^{(t)} = S_{12}^{(1)} DES_{12}^{(2)} \tag{13b}$$

$$S_{21}^{(t)} = S_{21}^{(2)} DFS_{21}^{(1)} \tag{13c}$$

$$S_{22}^{(t)} = S_{22}^{(2)} + S_{21}^{(2)} DFS_{22}^{(1)} DS_{12}^{(2)} \tag{13d}$$

where

$$\begin{aligned} E &= (I - S_{22}^{(2)} DS_{22}^{(1)} D)^{-1} \\ F &= (I - S_{22}^{(1)} DS_{22}^{(2)} D)^{-1} \\ D &= \begin{bmatrix} D^h & 0 \\ 0 & D^e \end{bmatrix} \end{aligned} \tag{14}$$

and D^h and D^e are diagonal matrices whose diagonal elements are given by

$$D_{nn}^h = e^{-\jmath k_{y_{1n}}^h l}, \qquad D_{nn}^e = e^{-\jmath k_{y_{1n}}^e l}. \tag{15}$$

C. Transverse Resonance Condition and Eigenvalue Equation

Out of the uniform sections connecting the discontinuities, we choose the one having the smallest vertical dimension (with respect to the transverse resonance direction, and use $S^{(L)}$ and $S^{(R)}$ to indicate the overall scattering matrices of the cascaded discontinuities on its left and right side, respectively, as indicated in Fig. 5. The column vectors, $A^{(L)}$ and $B^{(L)}$, accounting for incident and reflected wave amplitudes, respectively, of matrix $S^{(L)}$ in the left end region, and vectors $A^{(R)}$ and $B^{(R)}$ of matrix $S^{(R)}$ in the right end region, are related through the two end boundaries, which may be an electric wall (short-circuited) or a magnetic wall (open-circuited), as follows:

$$\begin{aligned} A^{(L)} &= \mp D^{(L)} D^{(L)} B^{(L)}, \\ A^{(R)} &= \mp D^{(R)} D^{(R)} B^{(R)} \end{aligned} \tag{16}$$

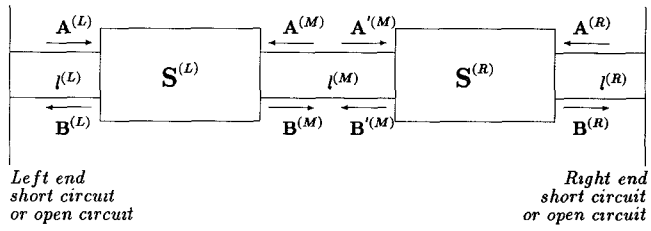

Fig. 5. Application of transverse resonance condition.

where the sign $\mp$ corresponds to the electric (upper one) and magnetic (lower one) wall, respectively. In the middle section, the forward and backward wave amplitudes are related by

$$\begin{aligned} A^{(M)} &= D^{(M)} B'^{(M)}, \\ A'^{(M)} &= D^{(M)} B^{(M)} \end{aligned} \tag{17}$$

where $A^{(M)}$ and $B^{(M)}$ are the amplitude column vectors of the incident and reflected modes, respectively, of matrix $S^{(L)}$ in the middle section, and $A'^{(M)}$ and $B'^{(M)}$ of matrix $S^{(R)}$. The diagonal elements in the diagonal matrices, $D^{(L)}, D^{(R)}$ and $D^{(M)}$, are defined in a similar way to that of (14) and (15), with the transverse propagation constant and propagation length l of the corresponding section.

Substituting (16) and (17) into the scattering matrix expressions of $S^{(L)}$ and $S^{(R)}$, the amplitude column vectors, $A^{(L)}, B^{(L)}, A^{(R)}, B^{(R)}, A^{(M)}$ and $A'^{(M)}$, may be eliminated, and $B^{(M)}$ and $B'^{(M)}$ are related by

$$B^{(M)} = (S_{21}^{(L)} E^{(L)} S_{12}^{(L)} + S_{22}^{(L)}) D^{(M)} B'^{(M)} \tag{18}$$

$$B'^{(M)} = (S_{21}^{(R)} E^{(R)} S_{12}^{(R)} + S_{22}^{(R)}) D^{(M)} B^{(M)} \tag{19}$$

where $E^{(R)}$ and $E^{(L)}$ are defined as

$$\begin{aligned} E^{(L)} &= \pm D^{(L)} D^{(L)} (I - S_{11}^{(L)} D^{(L)} D^{(L)})^{-1} \\ E^{(R)} &= \pm D^{(R)} D^{(R)} (I - S_{11}^{(R)} D^{(R)} D^{(R)})^{-1} \end{aligned}$$

For the existence of nontrivial solutions for the linear simultaneous equations, (18) and (19), the determinant should vanish, that is, the following eigenvalue equation should be solved

$$\operatorname{Det} G = 0 \tag{20}$$

where

$$\begin{aligned} G = I &- (S_{21}^{(L)} E^{(L)} S_{12}^{(L)} + S_{22}^{(L)}) D^{(M)} \\ &\cdot (S_{21}^{(R)} E^{(R)} S_{12}^{(R)} + S_{22}^{(R)}) D^{(M)} \end{aligned} \tag{21}$$

By using the transverse resonance condition at the section with the smallest vertical dimension, we obtain the final eigenvalue matrix G with the smallest size as the number of modal terms is the smallest in this region.

The commonly used transverse resonance procedure in other papers [7]–[11], on the contrary, is to treat the cascaded discontinuities from the left to the right or from the right to the left in sequence, and then to impose the two end boundary conditions. This procedure usually results in a large eigenvalue matrix since the two end sections are large in dimensions in most practical configurations.

Moreover, we may notice that as the coefficients of the mode functions in (5) are normalized, the elements in the scattering matrices, $S^{(L)}$ and $S^{(R)}$, are of order 1; and that the elements in the diagonal matrices $D^{(L)}, D^{(M)}, D^{(R)}$, exponentially decay (in the y-direction) for the evanescent LSE and LSM modes, so that the final eigenvalue matrix G in (21) is diagonal dominant with the diagonal elements of order 1. The reduced size of the eigenvalue matrix and the good property of the matrix elements enable the numerical computation process to be quite stable with the determinant of the eigenvalue matrix neither too large nor too small, thus greatly ease the numerical root searching process for eigenvalues. This is another merit of our method against the conventionally used transverse resonance process. Usually after several searching steps, the root of (20) may rapidly converge to results with good accuracy in the present method.

III. Numerical Results

The above stated process has been programmed for numerical calculation, and it has been checked against published data for various planar waveguides with rectangular conductor cross sections and for microstrip lines with trapezoidal cross section.

In Fig. 6(a), the propagation constant of the microstrip is shown as a function of frequency for trapezoidal conductor strips with corner angles α of 45° (underetched), 90° (rectangular), and 135° (electrolytic growth), respectively. Where available, the results are compared with those obtained by Railton and Mcgeehan [1], who used the finite-difference time-domain method (FDTD). While good agreement has been seen for $\alpha = 90°, 135°$, there is marked discrepancy for $\alpha = 45°$ at the high frequency end, where with the increase of frequency, the curve given by [1] did not rise smoothly but with a faster tendency towards crossing over the curve for $\alpha = 90°$. We consider this questionable and our results are more reliable. The calculation procedure of FDTD in [1] may need a larger number of nodes in order to ensure the convergence and the accuracy of its results.

So far the effect of the conductor strip cross section on higher order modes in microstrip lines has not been given by other authors. Here in Fig. 6(b), it is provided for the first higher order mode. As can be seen, the influence on the propagation constant is also pronounced and the single-mode bandwidth of the microstrip line varies for about 5 GHz.

Table I shows the convergence property of the effective dielectric constant of the dominant mode in the microstrip line with the number of division layers of the trapezoidal conductor strip ($\alpha = 135°$). We can see that a 3 or 4 layer divison yields converged results with satisfactory accuracy. As is well known, if the strip is extremely thin, the influence of its thickness on the propagation property of planar transmission lines will be very weak, so that usually a small number of divisions give converged results and further divisions make almost no contributions.

In Fig. 7, the effect of the metallization cross section on the propagation constant of finlines with mounting grooves is demonstrated. As can be seen, the discrepancy between the results of the two conductor profiles may be as large as 10%.

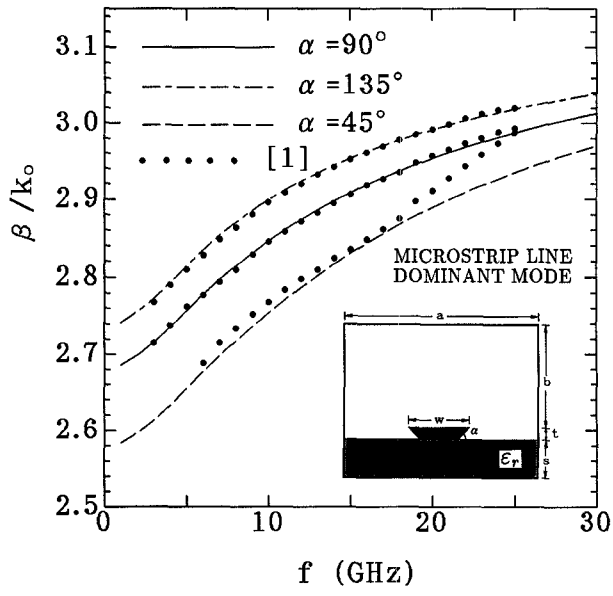

(a)

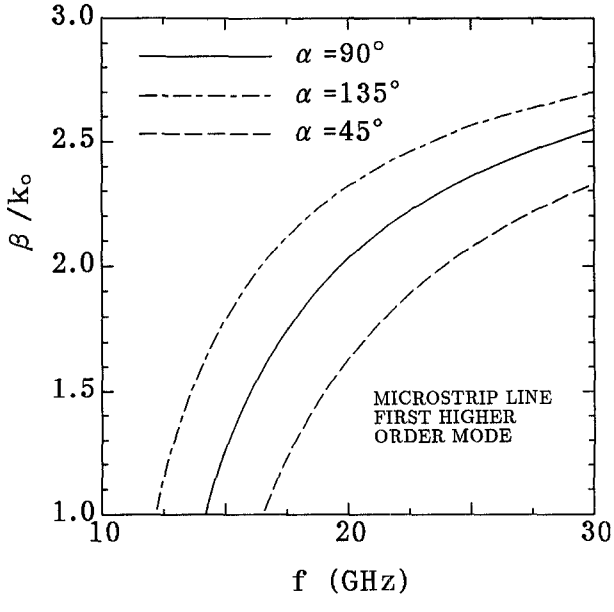

(b)

Fig. 6. Normalized propagation constant versus frequency for microstrips of various cross sections. (a) Dominant mode. (b) First higher order mode; $a = 10$ mm, $b = 6.05$ mm, $t = 300\,\mu$m, $s = 0.635$ mm, $w = 3$ mm, $\varepsilon_r = 9.8$.

TABLE I
Convergence Property of the E ffective Dielectric Constant of the Dominant Mode in the Microstrip Line with the Number of Division Layers of the Trapezoidal Conductor Strip ($\alpha = 135°$)

Number of Layers	Effective Dielectric Constants						
	1 GHz	5 GHz	10 GHz	15 GHz	20 GHz	25 GHz	30 GHz
2	2.73448	2.80811	2.89403	2.94949	2.98809	3.01626	3.03735
3	2.74168	2.81456	2.89911	2.95341	2.99107	3.01850	3.03903
4	2.74745	2.81981	2.90334	2.95674	2.99364	3.02048	3.04054
5	2.74769	2.81999	2.90346	2.95682	2.99371	3.02053	3.04058

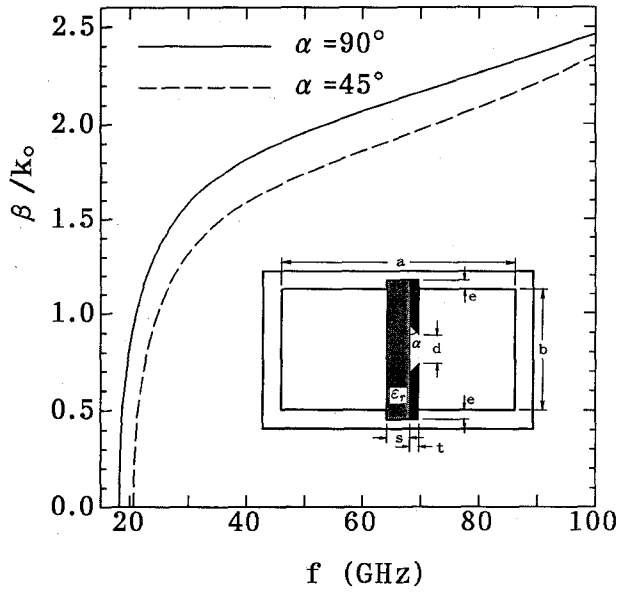

Fig. 7. Normalized propagation constant versus frequency for unilateral finlines of various cross sections; $a = 2b = 3.1$ mm, $d = 0.4$ mm, $e = 0.2$ mm, $s = 0.22$ mm, $t = 120\,\mu$m, $\varepsilon_r = 12.9$.

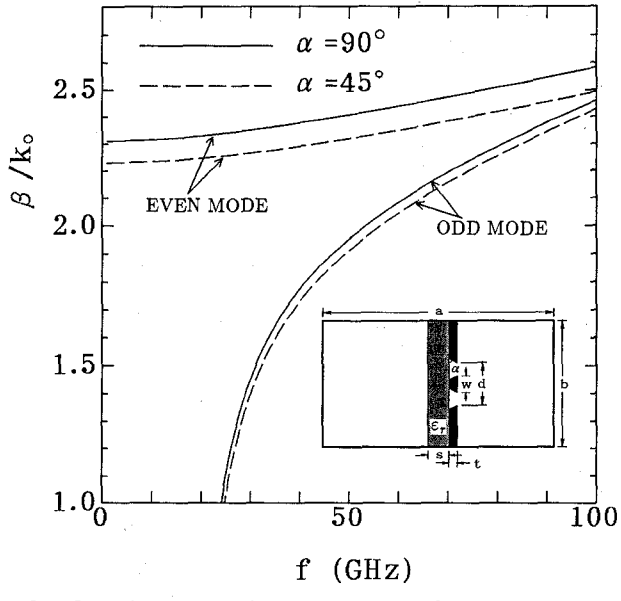

Fig. 8. Normalized propagation constant versus frequency for suspended coplanar waveguides of various cross sections; $a = 2b = 3.1$ mm, $d = 0.6$ mm, $w = 0.1$ mm, $s = 0.22$ mm, $t = 20\,\mu$m, $\varepsilon_r = 12.9$.

In the uniplanar MMIC concept [4], coplanar waveguides (CPW's) constitute the basic transmission line elements. Their cross sectional dimensions can be scaled down to values much smaller than those of the equivalent microstrip lines [4]–[6]. Because of the small cross sectional geometry, the CPW's are considerably less dispersive than the microstrip lines, and have an extended frequency range as well as a reduced circuit size. In Fig. 8, the propagation constants of both the dominant and the first higher order mode of a suspended coplanar waveguide (SCPW) are illustrated. While the geometry influence on the odd mode is negligible, it is, however, significant for the dominant mode over the whole frequency range.

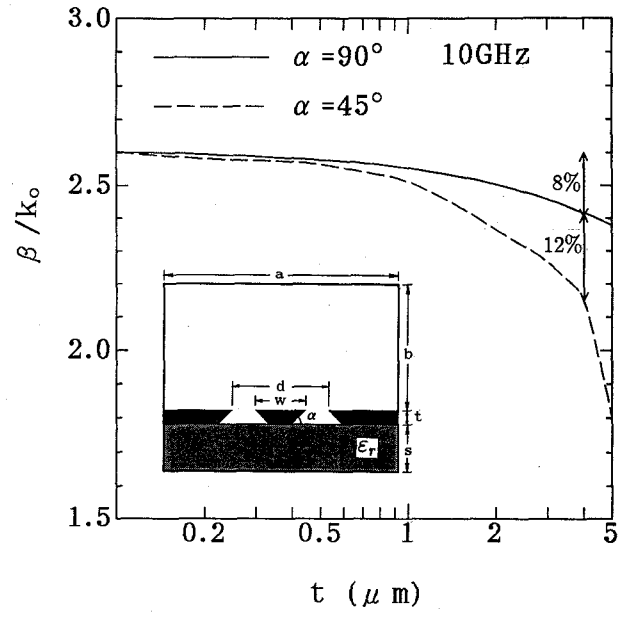

Fig. 9. Normalized propagation constant versus metallization thickness t for coplanar waveguides of various cross sections; $a = 150\,\mu$m, $b = 5$ mm, $s = 0.6$ mm, $d = 50\,\mu$m, $w = 10\,\mu$m, $\varepsilon_r = 12.9$.

Miniaturized CPW structures with width d of 30–70 μm are in use [5], [6]. For such miniaturized structures, we predict that the conductor profile will have even more pronounced effects on the transmission characteristics. To give an example, we provide in Fig. 9 the data on the propagation constants of a CPW with $d = 50\,\mu$m and center strip width 10 μm for different metallization thickness t. As expected, for extremely thin metallization, the influence of both its thickness and its profile is negligible, however, as the metallization thickness t becomes larger, the influence of its profile grows rapidly. For example, the discrepancies between results for $t = 4\,\mu$m and that for zero metallization thickness, are about 8% and 20% for the rectangle and the trapezoid, respectively. Also we note that the discrepancy between the latter two is about 12%. In such cases, it is certain that the effect of the metallization cross sections can no longer be neglected in order to obtain accurate and reliable predictions of performances of MMIC's.

IV. Conclusion

An analysis method has been proposed for planar waveguides with arbitrary metallization cross sections, and computations have been performed for various kinds of structures, which prove that the method is versatile and efficient. Numerical results indicate that, in the development of modern MMIC structures, which is towards higher frequencies and miniaturized sizes, the role of the metallization geometry becomes more and more important, and the exact modeling of practically used configurations is necessary so that accurate and reliable performance can be expected.

References

[1] C. J. Railton and J. P. Mcgeehan, "An analysis of microstrip with rectangular and trapezoidal conductor cross section," *IEEE Trans. Microwave Theory Tech.*, vol. 38, pp. 1017–1022, Aug. 1990.

[2] W. Schroeder and I. Wolff, "A new hybrid mode boundary integral method for analysis of MMIC waveguides with complicated cross section," in *IEEE MTT-S Int. Microwave Symp. Dig.*, Long Beach, CA, 1989, pp. 711–714.
[3] K. A. Michalski and D. Zheng, "Rigorous analysis of open microstrip lines of arbitrary cross-section in bound and leaky regimes," in *IEEE MTT-S Int. Microwave Symp. Dig.*, Long Beach, CA, 1989, pp. 787–790.
[4] T. Hirota, Y. Tarusawa, and H. Ogawa, "Uniplanar MMIC hybrids—A proposed new MMIC structure," *IEEE Trans. Microwave Theory Tech.*, vol. MTT-35, pp. 576–581, June 1987.
[5] M. Aikawa, H. Ogawa, and T. Sugeta, "MMIC progress in Japan," in *IEEE Microwave and Millimeter-Wave Monolithic Circuits Symp. Dig.*, 1989, pp. 1–6.
[6] D. S. Phatak, N. K. Das and A. P. Defonzo, "Dispersion characteristics of optically excited coplanar striplines: Comprehensive full-wave analysis," *IEEE Trans. Microwave Theory Tech.*, vol. 38, pp. 1719–1730, Nov. 1990.
[7] R. Vahldieck, "Accurate hybrid-mode analysis of various finline configurations including multilayered dielectrics, finite metallization thickness, and substrate holding grooves," *IEEE Trans. Microwave Theory Tech.*, vol. MTT-32, pp. 1454–1460, Nov. 1894.
[8] J. Bornemann and F. Arndt, "Calculating the characteristic impedance of finlines by transverse resonance method," *IEEE Trans. Microwave Theory Tech.*, vol. MTT-34, pp. 85–92, Jan. 1986.
[9] R. R. Mansour and R. H. Macphie, "A unified hybrid-mode analysis for planar transmission lines with multilayer isotropic/anisotropic substrates," *IEEE Trans. Microwave Theory Tech.*, vol. MTT-35, pp. 1382–1391, Dec. 1987.
[10] A. T. Villeneuve, "Analysis of slotted, dielectrically loaded, ridged waveguide," *IEEE Trans. Microwave Theory Tech.*, vol. MTT-32, pp. 1302–1310, Oct. 1984.
[11] R. R. Mansour and R. H. Macphie, "An improved transmission matrix formulation of cascaded discontinuities and its application to E-plane circuits," *IEEE Trans. Microwave Theory Tech.*, vol. MTT-34, pp. 1490–1498, Dec. 1986.
[12] R. Mittra and S. W. Lee, *Analytical Techniques in the Theory of Guided Waves*. New York: Macmillan, 1971.

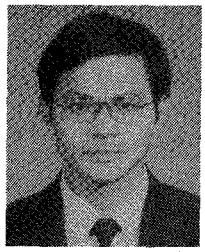

Zhewang Ma was born in Anhui, China, on July 7, 1964. He received the B.E. and M.E. degrees from the University of Science and Technology of China, Hefei, China, in 1986 and 1989, respectively, and is currently working towards the Ph.D. degree in the electronic engineering at the University of Electro-communications, Tokyo, Japan.

He has performed research works on dielectric waveguides and resonators, millimeter leaky-wave antennas. His present interests are in the analysis and design of microwave and millimeter-wave integrated circuits.

Eikichi Yamashita (M'66–SM'79–F'84), for a photograph and biography, see this issue, p. 483.

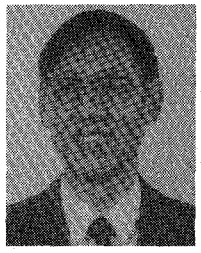

Shanjia Xu (SM'91) graduated from the University of Science and Technology of China in 1965.

Since then, he has been with the same university as a Professor and has been Associate Chairman of the Department of Radio and Electronics since 1986. From 1983 to 1986 he was a Visiting Scholar at the Polytechnic Institute of New York. During the winter of 1991, he was a Guest Scientist in Wurzburg University Germany. Also, he was an academic visitor at several universities in the United States, Canada, Japan, Germany and Hong Kong. He has been teaching microwave engineering courses for more than 25 years for graduate and undergraduate students. He has been engaged in research in the fields of microwave and millimeter-wave theory and techniques and has been participating in many research programs in cooperation with institutes and industrial laboratories. In addition, he has received the second and the third award for science and technology advances given by the Chinese Academy of Sciences.

He has published over 100 papers in various academic journals and proceedings of international conferences. His research interests are in the areas of nonuniform dielectric waveguides and applications, numerical techniques in electromagnetics and millimeter-wave technology. Mr. Xu is the Sub-Associate Editor of *IEEE, Microwave and Guided Wave Letters,* a member of the Editorial Board of the *Journal of Infrared and Millimeter Waves* and a standing member of the Editoral Board of the Journal of China Institute of Communications. He is Associate Chairman of the millimeter and submillimeter wave speciality of the Chinese MTT Society. His biography was listed in the *Who's Who of the Asian Pacific Rim.*